PCCP

COMMUNICATION

View Article Online
View Journal | View Issue

Cite this: *Phys. Chem. Chem. Phys.*, 2025, **27**, 20456

Received 28th June 2025,
Accepted 4th September 2025

DOI: 10.1039/d5cp02460a

rsc.li/pccp

Quantitative insights into the role of halogen and triel bonds in the formation of isostructural co-crystals of 4-iodophenyl boronic acid

Koushik Mandal, Ajay Suresh and Deepak Chopra *

Phenyl boronic acid, which exhibits structural similarity to carboxylic acid, forms a hydrogen-bonded homo-dimer. During the cocrystallization process, the hydrogen-bonded homodimer is often disrupted by the incorporation of coformers. In this study, we present two distinct cocrystals of 4-iodophenyl boronic acid: one with (iodoethynyl)benzene and the other with 1,4-diiodobenzene. Notably, in both cases, the hydrogen-bonded dimer remains unaffected. Instead, interactions between the coformers and 4-iodophenyl boronic acid are facilitated through halogen and triel bonds, and C–H···π interactions, resulting in the formation of isostructural solids. Furthermore, quantitative investigation of the halogen and triel bonds within the cocrystals was performed utilizing various approaches, including MESP, 2D fingerprint plot, 3D deformation density plot, QTAIM, and NBO analyses. These methods elucidate the intricate bonding interactions present in these systems, underscoring their complexity and significance.

1. Introduction

Cocrystallization serves as a valuable technique for enhancing the solid-state properties of parent compounds. This approach is particularly significant for compounds with practical applications, such as those found in the pharmaceutical industry.[1–4] The majority of knowledge-based research concerning cocrystals is based on two essential principles. The first was introduced by Etter in 1990[5] as the best proton donors and acceptors remaining after the formation of intramolecular hydrogen bonds form intermolecular hydrogen bonds. Desiraju introduced the second principle in 1995[6] as the idea of the supramolecular synthon as a robust and predictable intermolecular interaction in crystal engineering. In this context, the crystal engineering community has successfully harnessed homomeric and heteromeric intermolecular interactions involving carboxylic acids and carboxamides.[7,8] These interactions serve as effective tools for the predictable synthesis of crystalline materials.[9] Boronic acids are essential intermediates in the field of organic transformations and are recognized as key precursors in both bioorganic and medicinal chemistry.[10] Despite their potential, the utility of functional groups like boronic acids in solid-state non-covalent syntheses remains largely unexplored.[11]

Phenyl boronic acids are capable of existing in three distinct conformers: *syn–syn*, *syn–anti*, and *anti–anti*, each processing unique energy profiles. The relative stabilities of these conformers are quantified as follows: the *syn–anti* conformations exhibit an energy of 0.0 kcal mol^{-1}, while *syn–syn* is measured at 2.18 kcal mol^{-1} and *anti–anti* at 3.14 kcal mol^{-1}. In their native state, these compounds predominantly favor the energetically favourable *syn–anti* conformations.[12] However, in the context of a molecular complex, the compounds demonstrate conformational diversity (Scheme 1).

Theoretical calculations substantiate the premise that only energetically favourable synthons can facilitate the formation of heterosynthons.[12] Furthermore, both theoretical and structural analyses indicate that phenylboronic acids can engage with molecules in which heterocyclic and acidic fragments have the potential to disrupt the homosynthons.[12] Additionally,

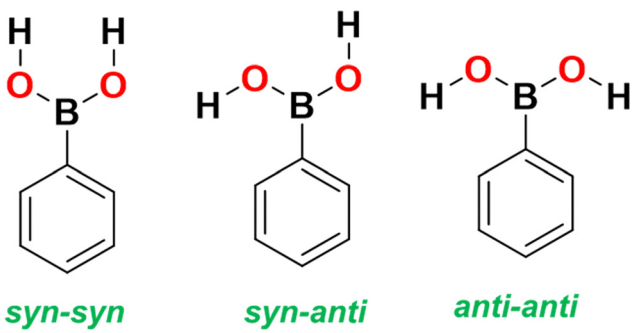

Scheme 1 Molecular conformations of phenyl boronic acid.

Crystallography and Crystal Chemistry Laboratory, Department of Chemistry, Indian Institute of Science Education and Research, Bhopal, Bhauri, Madhya Pradesh, 462066, India. E-mail: dchopra@iiserb.ac.in

three boronic acid units can undergo cyclodehydration, leading to the formation of a six-membered B_3O_3 (boroxine) ring.[13] Because of the conformational flexibility and the condensation product being a boroxine, it is always challenging to form cocrystals with phenyl boronic acid.

σ/π-hole based halogenated boronic acid cocrystals have not been explored yet, where, along with hydrogen bonds, halogen and other noncovalent interactions such as triel bonds help to bind coformers with boronic acid moieties. A halogen bond is formed when there is evidence of a net attractive interaction between an electrophilic region associated with a halogen atom in a molecular entity and a nucleophilic region in another, or the same, molecular entity.[14,15] Triel bonds are defined as interactions of the elements of the 13th group acting as the Lewis acid centres with the electron-rich regions that play the role of the Lewis base sites; they are usually classified as the π-hole bonds.[16,17]

A study utilizing the Cambridge Structural Database (CSD) was conducted to investigate the involvement of 4-iodophenyl boronic acid in the synthesis of cocrystals. The findings indicated that only four cocrystals featuring N-donor Lewis bases have been documented [Fig. S1(a) and (b)]. Subsequent structural analyses revealed that in all identified cocrystals, a homodimer formed *via* the boronic acid groups, which then converted into a heterodimer upon the incorporation of coformers (Fig. S1(c)).

In the present context, the formation of cocrystals (CC1 and CC2) is primarily attributed to the engagement of iodine-containing molecules, as depicted in Scheme 2 (dotted magenta box). These cocrystals are formed through halogen and triel bonds, while ensuring that the hydrogen-bonded homodimer remains undisturbed. Since the binding of coformers is facilitated *via* halogen and triel bonds to the 4-iodophenyl boronic acid, it is always fascinating to investigate the geometry and topological features associated with it.

2. Experimental

All the compounds, as mentioned in Scheme 2 and Scheme S1, were purchased from Sigma Aldrich and used directly without further purification. All potential combinations of substituted phenyl boronic acids and their corresponding co-formers were systematically evaluated for cocrystallization using the mechanochemical grinding method [Scheme S1]. This investigation consistently resulted in the formation of a boroxine moiety in nearly all cases, as experimental results, with the exceptions of cocrystals CC1 and CC2 [Scheme 2]. All the solvents used for the mechanochemical grinding and crystallization method are of analytical HPLC-grade only.

2.1. Preparation of cocrystals

2.1.1. CC1. Cocrystal CC1 was prepared *via* the solution crystallization method. 4-Iodophenyl boronic acid and (iodoethynyl)benzene (which is liquid at room temperature (RT)) were mixed in a 1 : 1 molar ratio in a round-bottom flask and stirred for approximately 4 hours in ethanol. The resulting solution was kept at room temperature (RT) for solvent evaporation. The final desired white product was crystallized in different polar solvents at low temperatures (4 °C). The plate crystals of CC1 were obtained in methanol and acetonitrile [Fig. S4(a)].

2.1.2. CC2. Cocrystal CC2 was prepared *via* the mechanochemical grinding method. 4-Iodophenyl boronic acid and

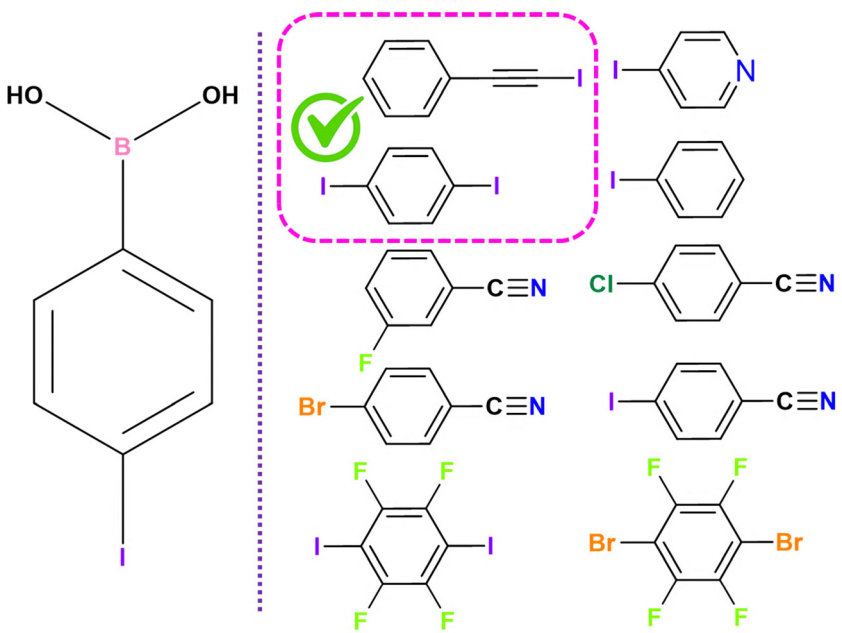

Scheme 2 Chemical scheme for co-crystal synthesis using substituted phenylboronic acids with different co-formers. The 4-iodophenylboronic acid and the co-formers mentioned in the magenta box are the successful combinations for the formation of co-crystals.

1,4-diiodobenzene were mixed in a 1 : 1 molar ratio in a mortar and ground with a pestle. After 15 minutes of neat grinding, 3 drops of methanol were added at an interval of 15 minutes (60 minutes), forming a fine white powder of CC2. This desired product was crystallized in different polar solvents at low temperatures (4 °C). The needle crystals of CC2 were obtained in methanol and nitromethane solvents [Fig. S4(b)], respectively.

3. Results and discussion

The synthesized products of CC1 and CC2 were characterized *via* powder X-ray diffraction (PXRD) and differential scanning calorimetry (DSC). Furthermore, the desired products were crystallized in a library of solvents using a slow evaporation method to get good-quality, suitable single crystals for single-crystal X-ray diffraction (SCXRD) to allow for the determination of the crystal structures (Fig. 1). The crystal packing was also performed for CC1 and CC2 using Mercury 4.0,[18] and the packing similarities were evaluated using the CSD material[19] present in Mercury. Furthermore, molecular electrostatic surface potential (MESP), 2D-fingerprint plots, and 3D deformation density plots were computed *via* Gaussian 09[20] and Crystal Explorer 21.5[21] to explore the quantitative nature and electrostatic complementarity of plausible noncovalent interactions (halogen and triel bonding synthons) associated with CC1 and CC2 cocrystals *via* a synthon-based approach. This was further supported *via* computations based on QTAIM[22] and NBO[23] methods.

3.1. Hirshfeld surface: molecular electrostatic surface potential (MESP)

The MESP of CC1 and CC2 was computed using Gaussian 09, utilizing the m062x and GENECP methods, to evaluate the surface potential of iodine σ-hole and lone pair regions along with the π-hole regions on B1 to B4 atoms and the respective phenyl regions as well [Fig. 2 and Table 1]. The computation was carried out using a split basis set obtained from the basis set library[24] (631-G(d,p) for C, H, B, and O, and LALN2DZD-P.ECP for the iodine atom). Those regions that can participate further in halogen and triel bonding interactions to form packing motifs are Motifs VII–XI and Motifs VII–XII in CC1 and CC2 cocrystals, respectively.

The σ-hole potential on the iodine atom (I5 : 84.8 kJ mol^{-1} for CC1; 76.2 kJ mol^{-1} for CC2) in both coformers is higher in comparison with all the other iodine atoms (I1 to I4) in 4-iodophenyl boronic acid [Fig. 2 and Table 1]. The σ-hole of I5 in CC1 exhibits a higher positive molecular electrostatic potential (MESP) of 84.8 kJ mol^{-1} compared to 76.2 kJ mol^{-1} for I5 in CC2. This difference arises because, in CC1, I5 is bonded to a –C≡C– (sp) group, which has greater electronegativity than the phenyl ring (sp^2) to which I5 is attached in CC2.

The positive MESP for the boron center is the highest for B4 in π4 for CC1 (80.0 kJ mol^{-1}) and CC2 (28.9 kJ mol^{-1}), respectively, signifying the most acidic center, of Lewis origin, in the respective cocrystals [Fig. 2 and Table 1]. Besides, the phenyl rings (M1 to M5 molecules), where the π-region of M1

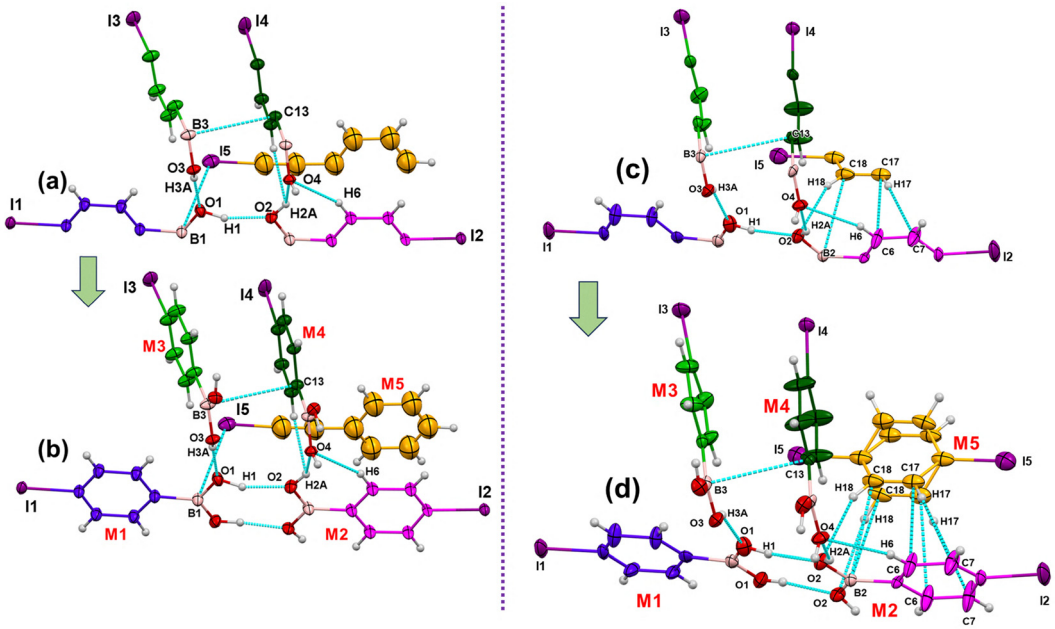

Fig. 1 Thermal ellipsoid plots (50% ellipsoidal probability) of (a) CC1 consisting of 4 half molecules of 4-iodophenyl boronic acid and 1 half molecule of (iodoethynyl)benzene, (b) CC1 cocrystal (dimer of the asymmetric unit, *via* crystallographic inversion center, composition: $C_{32}H_{29}B_4I_5O_8$), (c) CC2 consisting of 4 half molecules of 4-iodophenyl boronic acid and 1/4th molecule of 1,4-diiodobenzene, and (d) CC2 cocrystal (dimer of the asymmetric unit, *via* crystallographic inversion center, composition: $C_{54}H_{52}B_8I_{10}O_{16}$). The blue dotted lines depict the intermolecular interactions present in the asymmetric unit. In (b) and (d), the individual phenyl boronic acids are further assigned as M1 (blue), M2 (magenta), M3 (green), M4 (dark green), and M5 (orange), followed throughout the manuscript.

has the most negative potential (−61.8 kJ mol^{-1}) and M2 has the least (14.2 kJ mol^{-1}), are also present in CC1. So, the former acts as a strong electron donor, but the latter acts as a strong electron acceptor. But in CC2, the π-region of M4 acts as a strong electron donor (−45.1 kJ mol^{-1}), while M5 acts as a strong electron acceptor (27.2 kJ mol^{-1}) [Fig. 2 and Table 1].

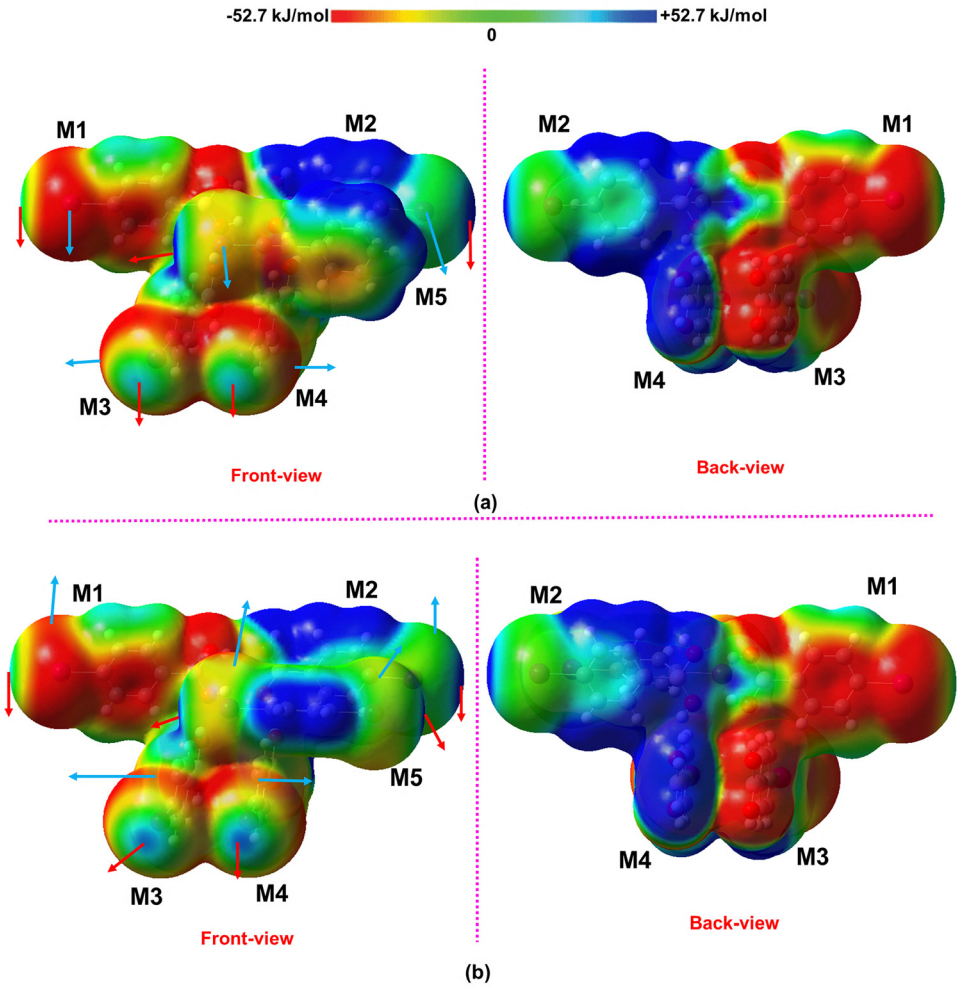

Fig. 2 MESP of cocrystals (a) CC1 (dimer of the asymmetric unit) and (b) CC2 (dimer of the asymmetric unit). The red and sky-blue arrows represent the MESP of the σ-hole and lone pair regions on iodine, respectively. The contour drawn for the MESP plot is in the range of −52.7 kJ mol^{-1} (red) to 0 (green) to +52.7 kJ mol^{-1} (blue). The corresponding MESP values are mentioned in Table 1.

Table 1 Important MESP values in kJ mol^{-1} for CC1 and CC2 cocrystals. Red and sky-blue arrows in Fig. 2 are iodine σ-hole and lone pair regions, respectively

Atoms/π(phenyl)	CC1 surface potential (kJ mol^{-1})		CC2 surface potential (kJ mol^{-1})	
I1	23.9(σ-hole)	−66.3(lone pairs)	43.2(σ-hole)	−51.7(lone pairs)
I2	75.4(σ-hole)	−43.0(lone pairs)	49.1(σ-hole)	−39.4(lone pairs)
I3	29.6(σ-hole)	−62.9(lone pairs)	40.9(σ-hole)	−53.9(lone pairs)
I4	28.2(σ-hole)	−47.3(lone pairs)	39.6(σ-hole)	−44.1(lone pairs)
I5	84.8(σ-hole)	−35.3(lone pairs)	76.2(σ-hole)	−18.8(lone pairs)
B1	11.3		28.7	
B2	83.2		9.2	
B3	6.91		6.8	
B4	80.0		28.9	
M1(ring)	−61.8		−42.7	
M2(ring)	14.2		22.2	
M3(ring)	−61.3		−44.4	
M4(ring)	−17.9		−45.1	
M5(ring)	−40.4		+27.2	

In the case of CC1, the phenyl ring of M1 and M2 shows electrostatic complementarity, suitable for stacking formation, and similar observations were also observed in CC2 [Fig. 2(a) and (b): back view; (Table 1)]. All the halogen bonds (I···I/π) and triel bonds (B···I/π) observed in the crystal packing, depicting electrostatic complementarity (Table 1), are discussed in the latter section.

3.2. Crystal packing of CC1 and CC2

The molecular arrangement of 4-iodophenyl boronic acid in CC1 and CC2 was consistent, with the coformer changed from (iodoethynyl)benzene to 1,4-diiodobenzene. CC1 and CC2 are isostructural[25–27] based on similar unit cells and the same space group, along with the same molecular arrangement of 4-iodophenyl boronic acid, where M1 and M2 molecules form hydrogen-bonded dimers (parallel to each other), which are perpendicular to the hydrogen-bonded dimers formed *via* M3 and M4 [Fig. 3(a) and (b)]. In M1 and M4, the boronic acid hydrogens are in a *syn–syn* conformation, whereas the acid hydrogens in M2 and M3 are in an *anti–anti* conformation, which is suitable for dimer formation.

In CC1, the hydrogen-bonded dimers formed *via* the O1–H1···O2 interaction (Motif I), consisting of M1 and M2 molecules, are parallel to each other, further supported *via* (C7)π···π(C3)/B1(π-hole)···π(C5) (Motif III) interactions to form a stack. Besides, the hydrogen-bonded dimers formed *via* the O4–H4···O3 interaction (Motif II), consisting of M3 and M4 molecules, are parallel and further connected *via* (C10)π···π(C15)/B3(π-hole)···π(C13) (Motif IV) interactions to form a stack. Two such stacks are orthogonal to each other and are further connected *via* O3–H3A···O1 (Motif V) and O2–H2A···O4 (Motif VI) interactions to form a chain when viewed in the *ab* plane [Fig. 3(a)]. In CC2, a similar chain is formed *via* similar interactions [Fig. 3(b)]. In the case of CC1, two such chains are connected *via* C1–I1(σ-hole)···π(C13) (shortening of XB: ∼6%, Motif VIII) interactions to form a 2D sheet when viewed in the *ab* plane [Fig. 3(c)], while in CC2, the chains are further connected *via* C1–I1(lp)···B3(π-hole) (Motif XI) interactions to form a 2D sheet [Fig. 3(d)].

Furthermore, an overlay diagram, consisting of fifteen molecules of 4-iodophenyl boronic acid in CC1 (gray) and CC2 (green), respectively, using Mercury[19] depicted that 14 out of 15 molecules exhibit similarity, with the RMSD value being 0.174 Å. Thus, the packing was established to be isostructural in nature [Fig. 3(e)].

For CC1, the discrete motif was formed *via* M5 with M4 and M3 respectively, through C15–H15···π(C22(sp)) and Type II C12–I3(lp)···I5(σ-hole)–C22 (shortening of XB: ∼4%) [Motif XII, X, Fig. 4(a)] interactions, which additionally stabilized the HB containing dimer (formed from M3 and M4) [Fig. 4(a)].

In Fig. 4(b), the stack formed [C5(π)···B1(π-hole) interactions, Motif III] *via* two such parallel M1 and M2 molecules containing the HB dimer is connected with M5 molecules through C22–I5(lp)···B1(π-hole) (Motif XI) (Fig. 4(b)) interactions to form a layer along the *c*-axis. Two similar layers are connected in a zig-zag way *via* the stack [C13(π)···B3(π-hole)

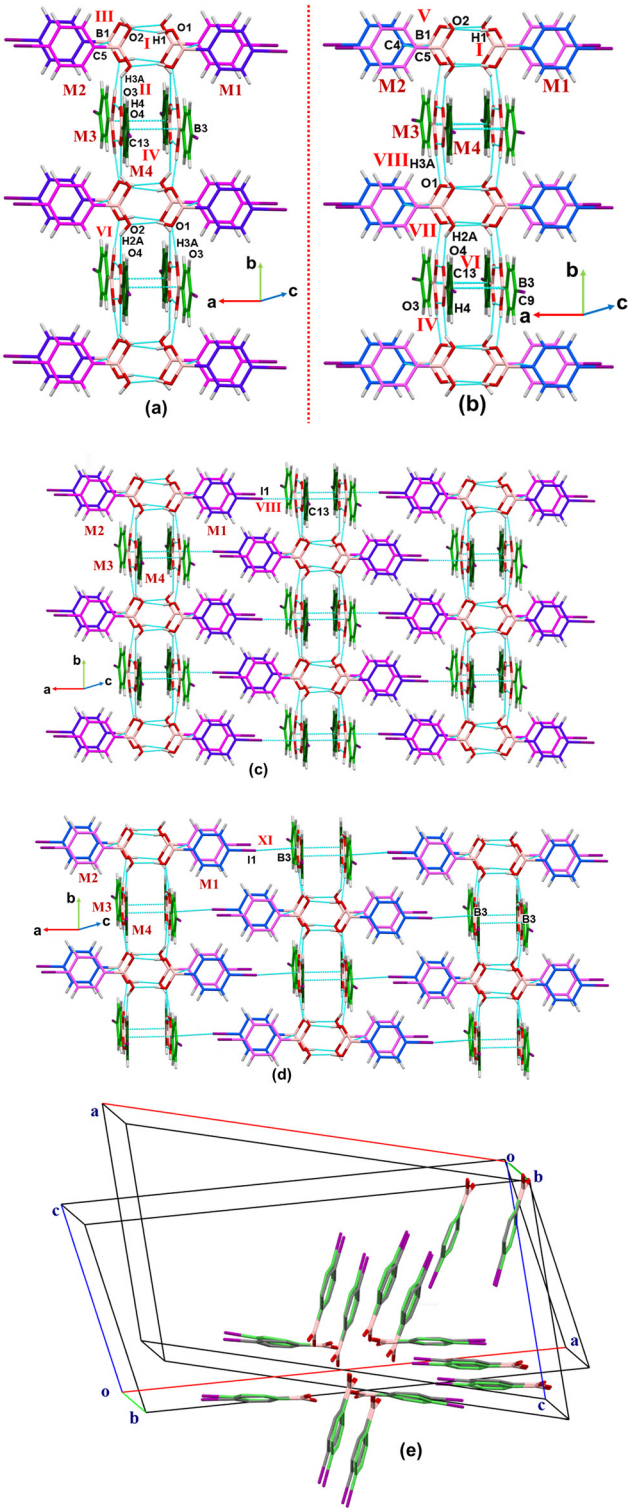

Fig. 3 Molecular arrangement of hydrogen-bonded dimers in 4-iodophenyl boronic acid present in both (a) and (c) CC1 and (b) and (d) CC2, and (e) overlay of crystal packing, consisting of 4-iodophenyl boronic acid only, present in CC1 (gray) and CC2 (green), respectively.

interactions, Motif IV], consisting of M3 and M4 molecules, containing the HB dimer motif, connected *via* C8–I2(lp)···B3 (π-hole) (shortening of triel bond (TB): ∼8%, Motif VII),

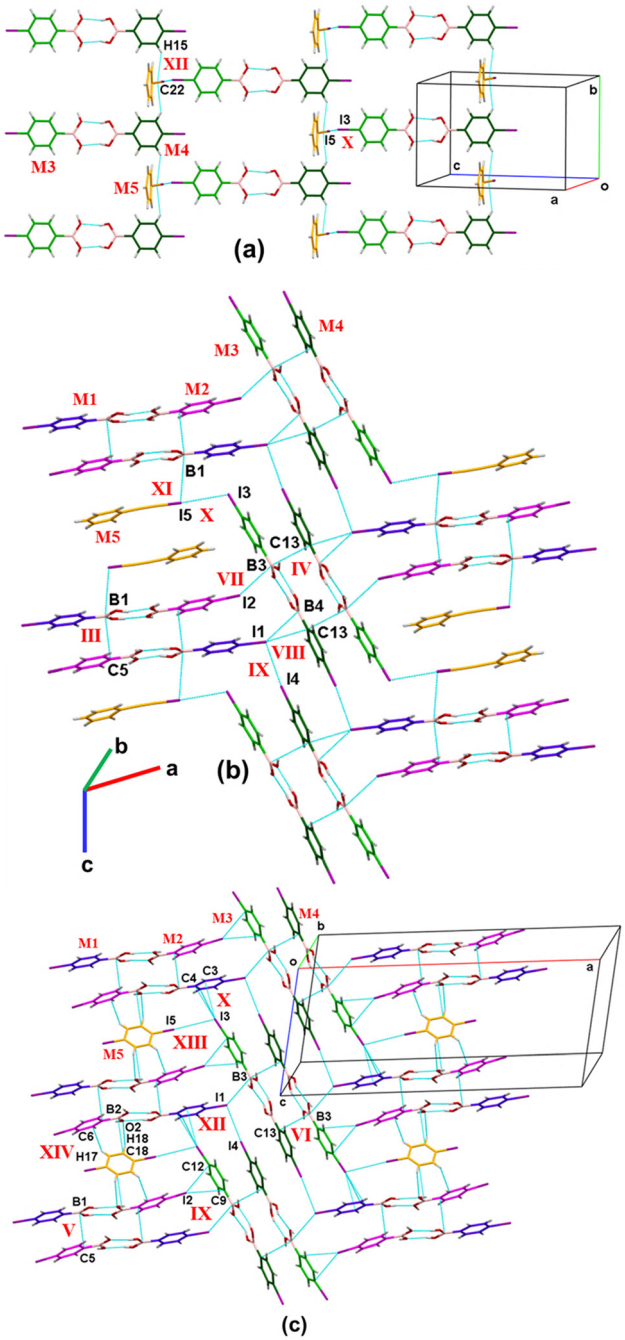

Fig. 4 Crystal packing of (a) and (b) CC1 in the *bc* and *ac* planes, respectively, and (c) CC2 in the *ac* plane.

C4–I1(σ-hole)···π(C13) (shortening of XB: ∼6%, Motif VIII), and Type II C4–I1(lp)···I4(σ-hole)–C22 (shortening of XB: ∼6%, Motif IX) interactions (Fig. 4(b)) in the *ac* plane.

In the case of CC2, the coformer (M5) interacted *via* C18–H18···O2, (C18)π···B2(π-hole), C17–H17···π(C6) (Motif XI) and Type II C19–I5···I3–C12 (Motif XIII) interactions with the stack [C5(π)···B1(π-hole) interactions, Motif V] consisting of M1 and M2 molecules containing the HB dimer motif, forming a layer in the *ac* plane [Fig. 4(c)]. Two similar layers are connected *via* C8–I2(σ-hole)···π(C12/C9) (elongation of XB: ∼1.4–2%, Motif IX), C12–I3(σ-hole)···π(C3/C4) (elongation of XB: ∼1.2–2%, Motif X), C1–I1(lp)···I4(σ-hole)–C16 (shortening of XB: ∼2.5%, Motif XII), and C12–I3(lp)···I5(σ-hole)–C19 (elongation of XB: ∼6%, Motif XII) in a zig-zag way, as demonstrated in Fig. 4(c).

In the crystal packing of CC1, two coformers (M5) were sandwiched between the stacks, whereas in CC2, only one coformer (M5) was sandwiched between the stacks to form a layer.

Furthermore, the halogen and triel bonding motifs present in both CC1 and CC2 cocrystals were subjected to in-depth analysis *via* the Quantum Theory of Atoms in Molecules (QTAIM) and Natural Bond Orbital (NBO) analyses as well. This comprehensive assessment underscores the intricate bonding interactions within these systems.

4. Computational study of halogen and triel bonds associated with the crystal packing of CC1 and CC2

The crystal packing analysis of CC1 and CC2 demonstrates the role of halogen and triel bonds, responsible for the binding of coformers to 4-iodophenyl boronic acid. Furthermore, all the halogen and triel bonding motifs and the corresponding non-covalent interactions present in these were extracted from the experimental crystal structures [(Motif VII–XI for CC1 and Motif XI-XIV for CC2) (Table 2)] and were subjected to different computational methods, as discussed below.

4.1. Quantum theory of atoms in molecules (QTAIM)

The existence of the triel and halogen contacts in CC1 and CC2 was further confirmed by the presence of a bond critical point (3, −1) and a bond path between the two interacting atom sites utilizing the m062x and GENECP methods. The computation was carried out using a split basis set obtained from the basis set library (631-G(d,p) for lighter atoms C, H, B, and O, and LALN2DZDP.ECP for the iodine atom).

For Motifs III, IV, and XI in CC1, no BCP was observed for boron-centered contacts, namely B1···π(C5), B3···π(C13), and B1···I5 respectively. Instead, the (C7)π···π(C3) and (C10)π···π(C15) contacts associated with the corresponding motifs showed the presence of a (3, −1) BCP. Similar observations were made for the boron-centered contacts in CC2 (Motifs V and VI). It is the π···π interactions that contribute to the crystal packing, instead of triel contacts, particularly in the case of the abovementioned motifs.

In CC1, the coformer was bound to boronic acid *via* Type II I···I contact [Motifs IX and X; Fig. 5(a) and (b)] wherein the values of ρ are in the range of 0.06–0.07 e Å^{-3}, and for the $\nabla^2\rho$, it is in the range of 0.62–0.74 e Å^{-5}. For CC2 [Motifs XII and XIII; Fig. 5(c) and (d)], the values of ρ and $\nabla^2\rho$ for the Type II I···I contact are in the range of 0.03–0.05 e Å^{-3} and 0.28–0.54 e Å^{-5}, respectively (Table 3). In CC1, the bond path length (R_{ij}) for the I4···I1 contact is 3.492 Å, which is shorter than that for the I5···I3 contact, with the magnitude being 3.574 Å.

Table 2 Intermolecular interactions in CC1 and CC2. The brown-shaded motifs are further discussed in the later sections as halogen and triel bonding motifs. Hydrogen, halogen, and triel bonds are referred to as HB, XB, and TB, respectively. The neutron-normalized values are reported for H-bonding contacts

Motif	Nature of contact [a]	Interactions A-B···D	Symmetry code	A···D (Å)	B···D (Å)	A-B···D/ B···D-E (°)
CC1						
I (M1···M2)	HB	O1-H1···O2	x, y, z	2.698(1)	1.79	163
II (M3···M4)	HB	O4-H4···O3	-x+1, -y+1, -z+2	2.7132(1)	1.80	163
III (M1···M2)	π···π/TB	(C7) π···π (C3)/B1···π (C5)	-x+1, y, -z+2	3.614(2)/3.434(2)	-	-
IV (M3···M4)	π···π/TB	(C10) π···π (C15)/ B3···π (C13)	x, y, z	3.664(2)/3.451(2)	-	-
V (M1···M3)	HB	O3-H3A···O1	x, y, z	2.637(1)	1.75	157
VI (M2···M4)	HB	O2-H2A···O4	x, y, z	2.724(1)	1.97	136
VII (M2···M3)	TB	C8-I2···B3	x+1/2, +y-1/2, +z	3.5636(2)	-	150, 105
VIII (M1···M4)	XB	C4-I1···π (C13)/B4	x-1/2, +y-1/2, +z	3.4428(3)/3.6068(2)	-	170, 93 144, 71
IX (M1···M4)	XB	I1···I4	-x+1/2, +y+1/2, -z+1	3.7037(2)	-	174, 100
X (M5···M3)	XB	I5···I3	-x+1/2, +y-1/2, -z+1	3.7972(2)	-	177, 108
XI (M5···M1)	TB	C22-I5···B1	x-1/2, +y-1/2, +z	3.916(5)	-	103, 102
XII (M5···M4)	HB	C15-H15···π (C22)	x, y, z	3.719(1)	2.92	143
CC2						
I (M1···M2)	HB	O1-H1···O2	x, y, z	2.717(4)	1.81	163
II (M1···M2)	HB	O1-H1···O2	x, -y, +z	3.574(4)	2.79	141
III (M4···M3)	HB	O4-H4···O3	-x+1, +y, -z	2.750(3)	1.88	153
IV (M4···M3)	HB	O4-H4···O3	-x+1, -y+1, -z	3.601(3)	2.84	139
V (M1···M2)	π···π/TB	(C4) π /B1···π (C5)	-x+1, +y, -z	3.779(4) 3.541(5)	-	-
VI (M4···M3)	π···π /TB	(C9) π /B3···π (C13)	x, y, z	3.730(1) 3.440(1)	-	-
VII (M2···M4)	HB	O2-H2A···O4 C6-H6···O4	x, y, z	2.726(3) 3.517(3)	1.90 2.48	146 161
VIII (M3···M1)	HB	O3-H3A···O1	x, y, z	2.642(7)	1.97	137
IX (M2···M3)	XB	C8-I2···π (C12/C9)	x-1/2, +y-1/2, +z	3.735(4)/3.757(5)	-	148, 109 167, 111
X (M3···M1)	XB	C12-I3···π (C3/C4)	-x+1/2+1, +y+1/2, -z+1	3.755(4)/3.724(4)	-	157, 78 177, 110
XI (M1···M3)	TB/XB	C4-I1···B3/O3	-x+1/2+1, +y-1/2, -z	3.745(1)/3.701(4)	-	142, 112 148, 81
XII (M1···M4)	XB	I1···I4	-x+1/2+1, +y-1/2, -z+1	3.859(5)	-	176, 97
XIII (M5···M3)	XB	I5···I3	x-1/2, +y-1/2, z	4.210(1)	-	177, 106
XIV (M4···M2)	HB/TB	C18-H18···O2 C17-H17···π (C6) (C18) π···B2	x, y, z	3.578(5) 3.511(1) 3.445(5)	2.56 2.67 -	157 148 -

[a] All the XB (I···I and I···π) contacts are lone pairs (I) → σ-hole (I) and (C) π → σ-hole (I) interactions respectively. All the TB contacts (I···B and B···π) are lone pairs (I) → π-hole (B) and (C) π → π-hole (B) interactions respectively.

The corresponding values, for R_{ij}, in CC2, for I4···I1 and I5···I3 contacts are 3.648 Å and 3.979 Å, respectively. Thus, an increase in the R_{ij} results in a decrease in the magnitude of ρ and $\nabla^2\rho$ at the BCPs. The internuclear separation also supports the trends in R_{ij} values in CC1 and CC2, respectively (Table 2). The range of magnitudes of the dissociation energy (based on V_b) is −4.88 to −6.19 kJ mol^{-1}, for the I···I contacts in CC1, which is greater than the corresponding values for the I···I contacts present in CC2 (−2.11 to −4.35 kJ mol^{-1}) (Table 3).

The electrostatic complementarity from MESP calculations for the I5···I3 contact is higher when compared to the I4···I1 contact (Table 1), which is similar to the case of CC2. Furthermore, it is interesting to note that the electrostatic complementarity of all I···I contacts present in CC1 is greater than that in CC2, which supports the higher magnitude of the bond dissociation energy of the former in comparison with the latter (Table 3).

The magnitudes of ρ and $\nabla^2\rho$ for the I···π contact in CC1 and CC2 are 0.06 e Å^{-3}, 0.66 e Å^{-5} and 0.04 e Å^{-3}, 0.39–0.41 e Å^{-5} respectively. The R_{ij} for the I1···π(C13) [Motif VIII; Fig. 5(e)] contact in CC1 is 3.233 Å, which is shorter than the I2···π(C12/C9) and I3···π(C3/C4) contacts [Motifs IX and X; Fig. 5(f) and (g)] present in CC2. The values are 3.539(I2···C9) Å/ 3.566(I2···C12) Å and 3.533(I3···C4) Å/3.682(I3···C3) Å, respectively. The I1···π(C13) contact in CC1 shows a greater magnitude of dissociation energy (−5.40 kJ mol^{-1}) as compared to the I···π contacts present in CC2 (−3.29 to −3.56 kJ mol^{-1}) (Table 3). Here also, the topological parameters, such as the lower bond path length (R_{ij}), are characterized by high values of ρ and $\nabla^2\rho$, which result in higher bond dissociation energies for the I···π contacts in CC1 in comparison with those in CC2 (Table 3).

The triel bonds formed between M3 and M2 molecules present in CC1 showed the presence of a BCP for the B3···I2 contact (0.04 e Å^{-3}, 0.48 e Å^{-5}, and 3.431 Å) [Motif VII, Fig. 5(h) and Table 3], wherein the triel contact, B3···I1 observed in the crystal packing of CC2, is a consequence of the adjacent I1···O3 contact [Motif XI, Fig. 5(i)]. It is to be noted that no BCP and bond path length were observed for this triel contact (Tables 2 and 3).

Overall, cocrystal CC1 is formed *via* halogen bonds and triel bonds, while halogen bonds are responsible for the formation of CC2, which was supported by the presence of BCPs and bond paths. The $|V_b|/G_b$ values for all contacts shown in Table 3 followed the Koch and Popelier criteria. Thus, these are closed-shell interactions.

4.2. Natural bond orbital (NBO) analysis

The stabilization energy $E^{(2)}$ associated with the delocalization from the donor NBO(i) to the acceptor NBO(j) is estimated as

$$E^{(2)} = \Delta E_{ij} = q_i F(i,j)^2/(\varepsilon_j - \varepsilon_i)$$

where $F(i, j)$ is the off-diagonal NBO Fock matrix elements, q_i is the donor occupancy, and "i" and "j" are the diagonal elements (orbital energies).

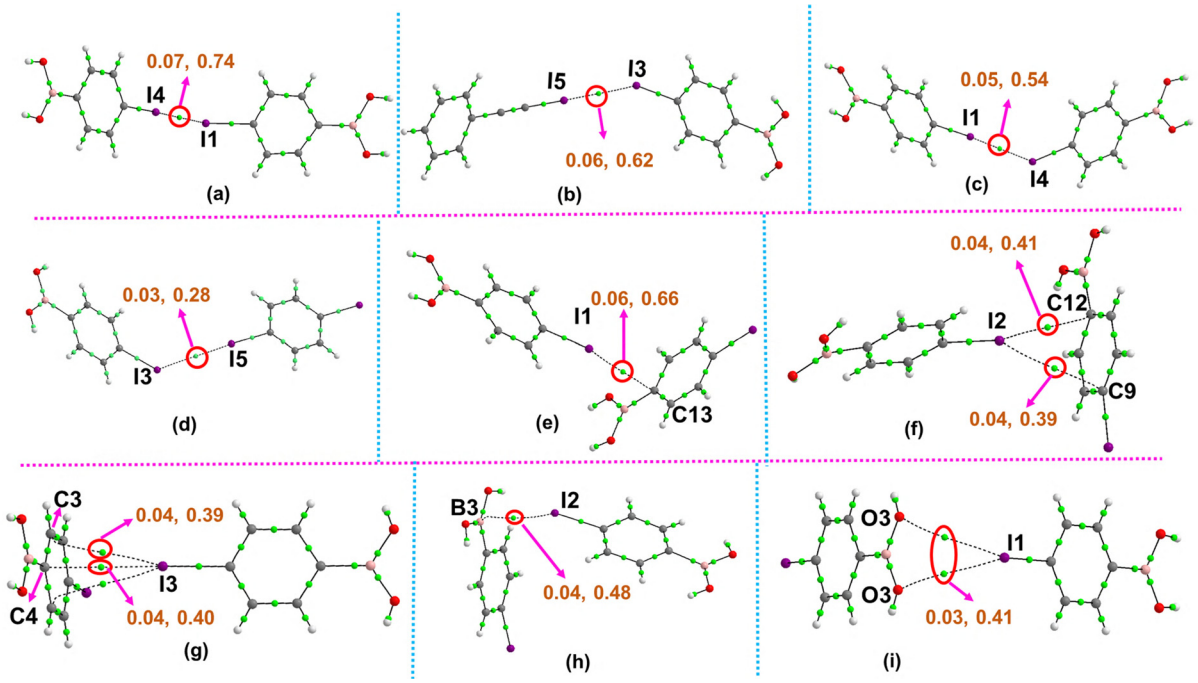

Fig. 5 Molecular graph for (a) Motif IX in CC1, (b) Motif X in CC1, (c) Motif XII in CC2, (d) Motif XIII in CC2, (e) Motif VIII in CC1, (f) Motif IX in CC2, (g) Motif X in CC2, (h) Motif VII in CC1, and (i) Motif XI in CC2, consisting of halogen and triel centered contacts, *via* the presence of (3, −1; green spheres) bond critical points (BCPs). BCPs (green spheres) are shown as red circles for noncovalent contacts, and the magenta arrow represents the corresponding ρ (e Å^{-3}) and $\nabla^2\rho$ (e Å^{-5}) values at BCPs. The dotted lines depict the bond paths.

Table 3 Topological parameters at the bond critical points (BCPs) for the different motifs present in CC1 and CC2

Cocrystal	Motif	Interactions	R_{ij} (Å)	ρ (e Å^{-3})	$\nabla^2\rho$ (e Å^{-5})	V_b (a.u.)	G_b (a.u.)	$\lvert V_b\rvert/G_b$	[a]D.E^V (kJ mol^{-1})
CC1	IX	I4···I1	3.492	0.07	0.74	−0.0047	0.0059	0.79	−6.19
	X	I5···I3	3.574	0.06	0.62	−0.0037	0.0049	0.76	−4.88
	VIII	I1···π(C13)	3.233	0.06	0.66	−0.0041	0.0053	0.77	−5.40
	VII	I2···B3	3.431	0.04	0.48	−0.0029	0.0039	0.74	−3.82
CC2	XII	I4···I1	3.648	0.05	0.54	−0.0033	0.0043	0.77	−4.35
	XIII	I5···I3	3.979	0.03	0.28	−0.0016	0.0022	0.73	−2.11
	IX	I2···π(C12)	3.566	0.04	0.39	−0.0025	0.0032	0.78	−3.29
		I2··· π(C9)	3.539	0.04	0.41	−0.0027	0.0035	0.77	−3.56
	X	I3··· π(C3)	3.682	0.04	0.39	−0.0025	0.0032	0.78	−3.29
		I3··· π(C4)	3.533	0.04	0.40	−0.0026	0.0033	0.79	−3.42
	XI	I1···O3	3.525	0.03	0.41	−0.0025	0.0034	0.74	−3.29

[a] D.E^V (kJ mol^{-1}) = $-0.5V_b \times 627.5 \times 4.2$; dissociation energy.[28] V_b is the local potential energy density at the BCP.

All the I···I contacts present in CC1 and CC2 (Motif IX, Motif X, Motif XII, and Motif XIII) [Fig. 6(a)–(d)] constitute orbital interactions of the n → σ* (I···I: 6.30–18.60 kJ mol^{-1}) origin. All the I···π contacts present in CC1 and CC2 (Motif VIII, Motif IX, and Motif X) [Fig. 6(e)–(g)] are orbital interactions of the π → σ* (I···π: 1.10–4.96 kJ mol^{-1}) origin. Motif VII [Fig. 6(h)] in CC1 corresponds to a triel bonding contact, as the electron density shifts from the I2(n) → B3(π*) orbital, with $E^{(2)}$ being 5.21 kJ mol^{-1} (Table S3). The I···O contact in CC2 [Fig. 6(i)] corresponds to the n → σ* orbital interaction with $E^{(2)}$ being 0.55 kJ mol^{-1} (Table S3). Overall, the formation of halogen and triel bonds was supported *via* NBO analysis, through the participation of orbital interactions. For I···I/π contacts, present in CC1 and CC2, the higher magnitudes of $E^{(2)}$ values, for the charge transfer interactions, are well corroborated with the magnitude of the topological parameters (*i.e.*, shorter R_{ij} and higher magnitudes of ρ and $\nabla^2\rho$).

Thus MESP, QTAIM and NBO calculations are extremely useful for understanding the complex electronic features of different non-covalent contacts observed in the cocrystal structures.

4.3. 3D-deformation density plot

A 3D-deformation density plot was computed to explore the charge-concentrated (CC) and charge-depleted (CD) regions on the corresponding atomic sites involved in halogen and triel bonding interactions in both CC1 and CC2. The calculations were performed at the B3LYP/DGDZVP level of theory.

All the halogen contacts, such as I···I, in cocrystals (Motifs IX and X: CC1; Motifs XII and XIII: CC2) [Fig. 7(a)–(d)] are

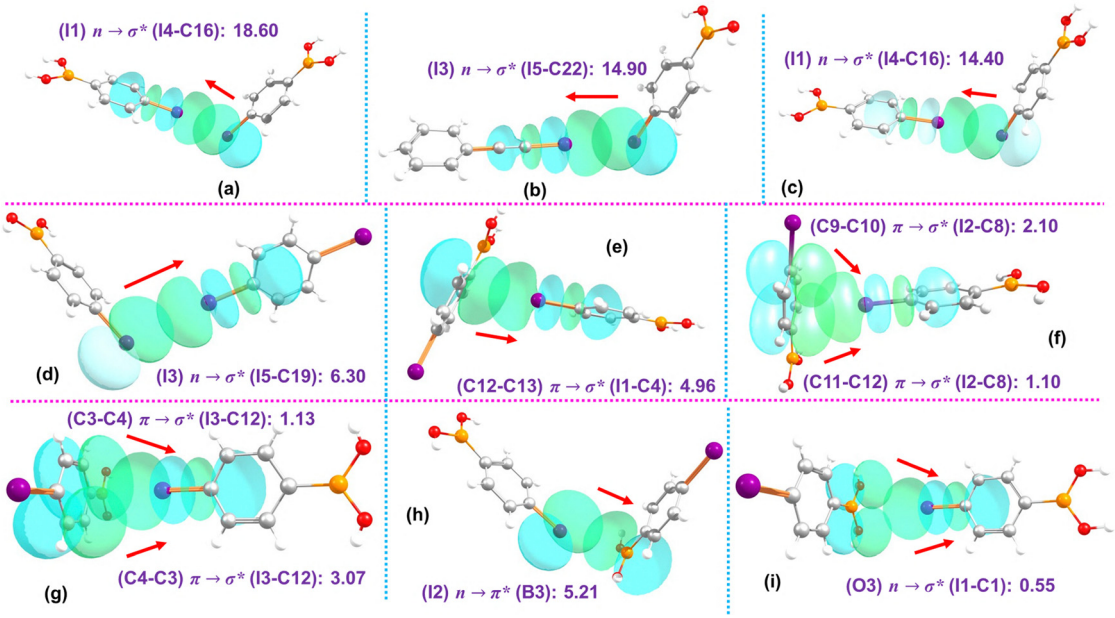

Fig. 6 Orbital interactions of the involved halogen and triel-centered contacts present in (a) Motif IX in CC1, (b) Motif X in CC1, (c) Motif XII in CC2, (d) Motif XIII in CC2, (e) Motif VIII in CC1, (f) Motif IX in CC2, (g) Motif X in CC2, (h) Motif VII in CC1, and (i) Motif XI in CC2. The red arrow indicates the electron density shift from the donor to the acceptor orbitals.

charge-concentrated (CC)···(CD) charge-depleted contacts. The triel contact as I···B (Motif VII: CC1) [Fig. 7(e)], in CC1, is a I(CC)···B(CD) contact. The I···O contact (Motif XI: CC2) [Fig. 7(f)] is an I(CD)···O(CC) contact.

4.4. 2D-finger print plots and contribution (%) of different intermolecular contacts

The contribution (%) of different intermolecular contacts (specifically, O···H/H···O, halogen, and triel contacts) was

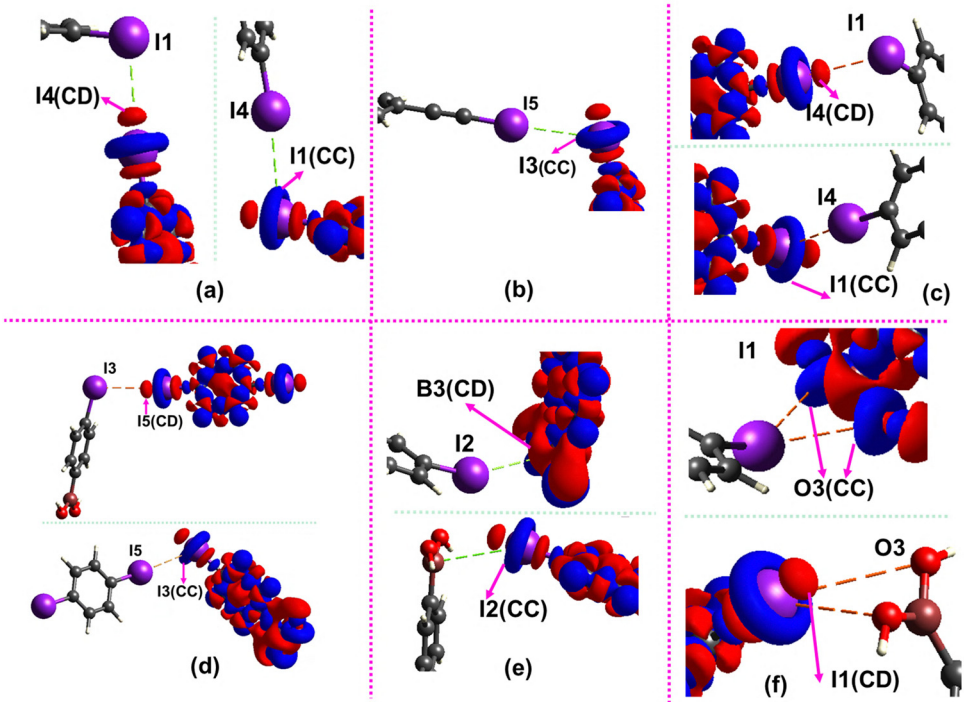

Fig. 7 3D-deformation density plot for the I···I contact in (a) Motif IX in CC1, (b) Motif X in CC1, (c) Motif XII in CC2, (d) Motif XIII in CC2, (e) I···B contact (Motif VII in CC1), and (f) I···O contact (Motif XI in CC2). CD and CC represent the charge-depleted (red) and charge-concentrated (blue) regions.

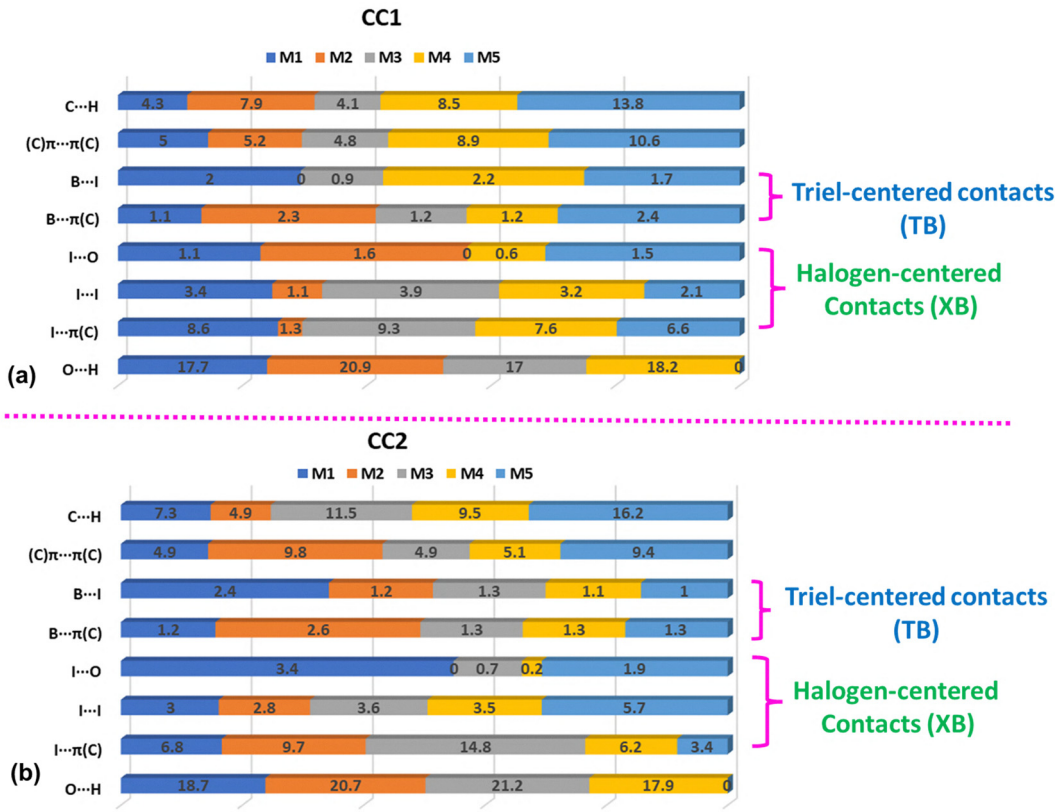

Fig. 8 Bar plots extracted from 2D-fingerprint plots showing the population of π···π, C–H···π, halogen, and triel-centered contacts for (a) CC1 and (b) CC2 cocrystals.

extracted from the 2D-fingerprint plots [Fig. 8 and Fig. S5]. In both co-crystals, the hydrogen-bonded dimer in 4-iodophenyl boronic acid remains unchanged. So, the % contribution of the O···H/H···O contacts (CC1: 17.7–20.9%, CC2: 17.9–21.2%) is similar for both cases. The % contributions of the I···π contact in M3 in CC1 and CC2 are the highest (9.3% and 14.8% respectively) and the % contribution of the I···I contacts in CC1 is the highest for M3 (3.9%), whereas it is the highest in M5 (5.7%) in CC2. However, along with halogen contacts, both the cocrystals are also cumulatively stabilized *via* triel contacts as the B···π/I contact. The % contributions of the B···π contacts in both cocrystals are (CC1: 1.1–2.4%, CC2: 1.2–2.6%) similar, whereas the % contribution of the B···I contact is higher in M4 (2.2%) in CC1. In CC2, it is the highest in M1 (2.4%). The % contribution of the I···O contact in CC2 is the highest for M1 (3.4%), whereas it is the highest in M2 (1.6%) in CC1. The % contribution of the π···π and H···π(C) contacts is the highest in M5 in CC1 (10.6%, 13.8%) and CC2 (9.4%, 16.2%) cocrystals.

5. Summary

It is well realized from the current study that the spontaneous formation of boroxine from the boronic acid residue makes the formation of cocrystals with substituted boronic acids difficult. However, in spite of this serious limitation, two cocrystals of 4-iodophenyl boronic acid with (iodoethynyl)benzene and 1,4-diiodobenzene coformers (CC1 and CC2) were successfully synthesized *via* solution crystallization after mechanochemical grinding. These were characterized both experimentally and the novel noncovalent interactions present within the crystal packing were characterized using different computational techniques. The hydrogen-bonded dimers formed between 4-iodophenyl boronic acids remain unchanged even after the incorporation of coformers, which leads to the formation of two isostructural solids. In this context, halogen and triel bonds (which took part in the binding of the coformers to the boronic acid moieties) were probed using MESP, QTAIM, and NBO methods along with the 3D-deformation density plots, to obtain quantitative and qualitative insights into the nature of halogen and triel bonds that characterizes the electronic features of these contacts in the solid state.

Author contributions

KM: investigation, methodology, validation, formal analysis, and writing the original draft. AS: investigation and validation. DC: conceptualization, resources, supervision, validation, and writing – review and editing.

Conflicts of interest

There are no conflicts to declare.

Data availability

The data supporting this article have been included as part of the SI. See DOI: https://doi.org/10.1039/d5cp02460a.

CCDC 2466139 and 2466140 contain the supplementary crystallographic data for this paper.[29a,b]

Acknowledgements

KM thanks IISER Bhopal for a research fellowship. KM, AS and DC thank IISER Bhopal for research facilities and research infrastructure.

References

1 G. Bolla and A. Nangia, Pharmaceutical Cocrystals: Walking the Talk, *Chem. Commun.*, 2016, **52**(54), 8342–8360.
2 N. K. Duggirala, M. L. Perry, Ö. Almarsson and M. J. Zaworotko, Pharmaceutical Cocrystals: Along the Path to Improved Medicines, *Chem. Commun.*, 2016, **52**(4), 640–655.
3 G. Bolla, B. Sarma and A. K. Nangia, Crystal Engineering of Pharmaceutical Cocrystals in the Discovery and Development of Improved Drugs, *Chem. Rev.*, 2022, **122**(13), 11514–11603.
4 K. Kopczyńska, C. J. Kingsbury, E. Pidcock, A. A. Moldovan and I. D. Madura, A Case of Unusual Cocrystal Polymorphs of Caffeine and Phenylboronic Acid: Cambridge Structural Database Tools in Action, *Cryst. Growth Des.*, 2024, **24**(12), 5159–5170.
5 M. C. Etter, Hydrogen Bonds as Design Elements in Organic Chemistry, *J. Phys. Chem.*, 1991, **95**(12), 4601–4610.
6 V. R. Thalladi, B. S. Goud, V. J. Hoy, F. H. Allen, J. A. K. Howard and G. R. Desiraju, Supramolecular Synthons in Crystal Engineering. Structure Simplification, Synthon Robustness and Supramolecular Retrosynthesis, *Chem. Commun.*, 1996, (3), 401–402.
7 J. A. Bis and M. J. Zaworotko, The 2-Aminopyridinium-Carboxylate Supramolecular Heterosynthon: A Robust Motif for Generation of Multiple-Component Crystals, *Cryst. Growth Des.*, 2005, **2**(8), 1169–1179.
8 J. Prakashareddy and V. R. Pedireddi, Synthesis and Analysis of Some Adducts of 3,5-Dinitrobenzamide, *Tetrahedron*, 2004, **60**, 8817–8827.
9 A. Cozzolino, C. Daniel and P. Rizzo, Monomeric and Dimeric Carboxylic Acid in Crystalline Cavities and Channels of Delta and Epsilon Forms of Syndiotactic Polystyrene, *Polym. J.*, 2021, **13**, 3330–3342.
10 D. G. Hall, *Ruthenium in Organic Synthesis Metal-Catalyzed Cross-Coupling Reactions Modern Rhodium-Catalyzed Organic Reactions Transition Metals for Organic Synthesis Asymmetric Organocatalysis*, WILEY-VCH Verlag GmbH & Co. KGaA, Weinheim, 2005.
11 V. Sunil, S. S. Bhushan and G. R. Desiraju, Phenylboronic Acids in Crystal Engineering: Utility of the Energetically Unfavorable *Syn*,*Syn*-Conformation in Co-Crystal Design, *Sci. China Inf. Sci.*, 2011, **54**(12), 1909–1919.
12 J. D. Larkin, K. L. Bhat, G. D. Markham, B. R. Brooks, H. F. S. Iii and C. W. Bock, Structure of the Boronic Acid Dimer and the Relative Stabilities of Its Conformers, *J. Phys. Chem. A*, 2006, **2**, 10633–10642.
13 K. L. Bhat, G. D. Markham, J. D. Larkin and C. W. Bock, Thermodynamics of Boroxine Formation from the Aliphatic Boronic Acid Monomers R–B(OH)$_2$ (R = H, H_3C, H_2N, HO, and F): A Computational Investigation, *J. Phys. Chem. A*, 2011, **2**, 7785–7793.
14 G. R. Desiraju, P. S. Ho, L. Kloo, A. C. Legon, R. Marquardt, P. Metrangolo, P. Politzer, G. Resnati and K. Rissanen, Definition of the Halogen Bond, *Pure Appl. Chem.*, 2013, **85**(8), 1711–1713.
15 C. Gabriella, M. Pierangelo, M. Roberto, P. Tullio, P. Arri, R. Giuseppe and T. Giancarlo, The Halogen Bond, *Chem. Rev.*, 2016, **116**, 2478–2601.
16 S. J. Triel Grabowski, Bond and Coordination of Triel Centres – Comparison with Hydrogen Bond Interaction, *Coord. Chem. Rev.*, 2020, **407**, 213171–213192.
17 E. C. Escudero-Adán, A. Bauzá, C. Lecomte, A. Frontera and P. Ballester, Boron Triel Bonding: A Weak Electrostatic Interaction Lacking Electron-Density Descriptors, *Phys. Chem. Chem. Phys.*, 2018, **20**(37), 24192–24200.
18 C. F. Macrae, I. Sovago, S. J. Cottrell, P. T. A. Galek, E. Pidcock, M. Platings, G. P. Shields, J. S. Stevens, M. Towler and P. A. Wood, Computer Programs Mercury 4 0: From Visualization to Analysis, Design and Prediction, *J. Appl. Crystallogr.*, 2020, **53**(1), 226–235.
19 A. Q. Meng, L. A. Diment, A. Abdi, V. J. Hubbs, E. A. Jeffreys, M. O. Dell, X. Ou, K. A. Park, B. T. Quillin and D. A. Dickie, Using Data from the Cambridge Structural Database to Practice Crystallographic Skills and Revise Erroneous Structures, *Cryst. Growth Des.*, 2024, **24**, 4690–4696.
20 M. J. Frisch, G. W. Trucks, H. B. Schlegel, G. E. Scuseria, M. A. Robb, J. R. Cheeseman, G. Scalmani, V. Barone, G. A. Petersson, H. Nakatsuji, X. Li, M. Caricato, A. Marenich, J. Bloino, B. G. Janesko, R. Gomperts, B. Mennucci, H. P. Hratchian, J. V. Ortiz, A. F. Izmaylov, J. L. Sonnenberg, D. Williams-Young, F. Ding, F. Lipparini, F. Egidi, J. Goings, B. Peng, A. Petrone, T. Henderson, D. Ranasinghe, V. G. Zakrzewski, J. Gao, N. Rega, G. Zheng, W. Liang, M. Hada, M. Ehara, K. Toyota, R. Fukuda, J. Hasegawa, M. Ishida, T. Nakajima, Y. Honda, O. Kitao, H. Nakai, T. Vreven, K. Throssell, J. A.Montgomery, G. E. Peralta, Jr., F. Ogliaro, M. Bearpark, J. J. Heyd, E. Brothers, K. N. Kudin; V. N. Staroverov, T. Keith, R. Kobayashi, J. Normand, K. Raghavachari, A. Rendell, J. C. Burant, S. S. Iyengar, J. Tomasi, M. Cossi, J. M. Millam, M. Klene, C. Adamo, R. Cammi, J. W. Ochterski, R. L. Martin, K. Morokuma, O. Farkas, J. B. Foresman and D. J. Fox, Gaussian, Inc., Wallingford CT, 2016.

21 P. R. Spackman, M. J. Turner, J. J. McKinnon, S. K. Wolff, D. J. Grimwood, D. Jayatilaka and M. A. Spackman, CrystalExplorer: A Program for Hirshfeld Surface Analysis, Visualization and Quantitative Analysis of Molecular Crystals, *J. Appl. Crystallogr.*, 2021, **54**(3), 1006–1011.

22 P. Popelier and C. Town, *Atoms in Molecules: An Introduction*, Prentice Hall, London. 2000.

23 (*a*) E. D. Glendening, C. R. Landis and F. Weinhold, Natural Bond Orbital Methods, *Comput. Mol. Sci.*, 2012, **2**, 1–42; (*b*) S. Scheiner, The Pnicogen Bond: Its Relation to Hydrogen, Halogen, and Other Noncovalent Bonds, *Acc. Chem. Res.*, 2013, **46**(2), 280–288.

24 B. P. Pritchard, D. Altarawy, B. Didier, T. D. Gibson and T. L. Windus, New Basis Set Exchange: An Open, Up-to-Date Resource for the Molecular Sciences Community, *J. Chem. Inf. Model.*, 2019, **59**, 4814–4820.

25 L. Fábián and A. Kálmán, Isostructurality in One and Two Dimensions: Isostructurality of Polymorphs, *Acta Crystallogr., Sect. B: Struct. Sci.*, 2004, **60**(5), 547–558.

26 T. Gelbrich, T. L. Threlfall and M. B. Hursthouse, XPac Dissimilarity Parameters as Quantitative Descriptors of Isostructurality: The Case of Fourteen 4,5′-Substituted Benzenesulfonamido-2-Pyridines Obtained by Substituent Interchange Involving CF3/I/Br/Cl/F/Me/H, *CrystEngComm*, 2012, **14**(17), 5454–5464.

27 P. Bombicz, What Is Isostructurality? Questions on the Definition, *IUCrJ*, 2024, **11**, 3–6.

28 (*a*) I. Mata, I. Alkorta, E. Espinosa and E. Molins, Relationships between interaction energy, intermolecular distance and electron density properties in hydrogen-bonded complexes under external electric fields, *Chem. Phys. Lett.*, 2011, **507**(1), 185–189; (*b*) S. Bhandary, A. Sirohiwal, R. Kadu, S. Kumar and D. Chopra, Dispersion Stabilized Se/Te$\cdots\pi$ Double Chalcogen Bonding Synthons in in Situ Cryocrystallized Divalent Organochalcogen Liquids, *Cryst. Growth Des.*, 2018, **18**(7), 3734–3739.

29 (*a*) K. Mandal, A. Suresh and D. Chopra, CCDC 2466139: Experimental Crystal Structure Determination, 2025, DOI: **10.5517/ccdc.csd.cc2ns6wk**; (*b*) K. Mandal, A. Suresh and D. Chopra, CCDC 2466140: Experimental Crystal Structure Determination, 2025, DOI: **10.5517/ccdc.csd.cc2ns6xl**.